Systems/Circuits

Optogenetic Assessment of Horizontal Interactions in Primary Visual Cortex

Xiaoying Huang,[1,2]* Yishai M. Elyada,[1,2]* William H. Bosking,[1] Theo Walker,[1] and David Fitzpatrick[1,2,3]

[1]Department of Functional Architecture and Development of Cerebral Cortex, Max Planck Florida Institute for Neuroscience, Jupiter, Florida 33458, [2]Department of Neurobiology, Duke University Medical Center, Durham, North Carolina 27710, and [3]Duke Institute for Brain Sciences, Durham, North Carolina 27710

Columnar organization of orientation selectivity and clustered horizontal connections linking orientation columns are two of the distinctive organizational features of primary visual cortex in many mammalian species. However, the functional role of these connections has been harder to characterize. Here we examine the extent and nature of horizontal interactions in V1 of the tree shrew using optical imaging of intrinsic signals, optogenetic stimulation, and multi-unit recording. Surprisingly, we find the effects of optogenetic stimulation depend primarily on distance and not on the specific orientation domains or axes in the cortex, which are stimulated. In addition, across a wide range of variation in both visual and optogenetic stimulation we find linear addition of the two inputs. These results emphasize that the cortex provides a rich substrate for functional interactions that are not limited to the orientation-specific interactions predicted by the monosynaptic distribution of horizontal connections.

Introduction

The columnar arrangement of neurons with similar response properties is a common feature of cortical organization in many mammals and is especially well developed in visual cortex (Hubel and Wiesel, 1977; Mountcastle, 1997, 2003). The similarity in the response properties that define neurons in a given cortical column is thought to derive from an underlying specificity in the arrangement of vertical and horizontal connections. Neurons in layer 2/3 receive feedforward inputs from a radially restricted population of layer 4 neurons (Fitzpatrick, 1996; Hirsch and Martinez, 2006). In carnivores, primates, and scandentia (tree shrews), recurrent horizontal connections extend for long distances (>2 mm) across the cortical surface and are distributed in a modular fashion that reflects a bias for columns that have similar response properties, such as selectivity for stimulus orientation (Gilbert and Wiesel, 1989; Malach et al., 1993; Bosking et al., 1997). This specificity in anatomical connections suggests that functional interactions between cortical columns would display a corresponding specificity. However, there are at least two caveats related to these anatomical studies. First, the exact tuning of the synaptic inputs that are supplied by horizontal inputs is unknown, and second, these studies emphasize the pattern of monosynaptic connections and may underestimate the full complexity of multisynaptic network interactions.

A number of optogenetic techniques are available that can more directly address these questions (Boyden et al., 2005; Fenno et al., 2011; Yizhar et al., 2011). Optogenetic experiments performed in tissue slices have examined functional organization of horizontal connections (Petreanu et al., 2007, 2009; Wang et al., 2007; Adesnik and Scanziani, 2010; Kätzel et al., 2011; Mao et al., 2011). However, tissue slices lack the full complement of intracortical connections and cannot be used to assess the involvement of these circuits in the generation of visually driven responses. Recently, these tools have also been used successfully to examine circuit specificity in rodents *in vivo* (Ayling et al., 2009; Hira et al., 2009; Harrison et al., 2012; Lim et al., 2012). However, these techniques have not been used to examine the full range and spatial organization of lateral interactions in visual cortex of species that have a systematic map of orientation preference.

In this study, we used a spatial light modulator to deliver patterns of blue light in register with a cortical orientation map acquired by optical imaging of intrinsic signals. This allowed us to selectively activate functionally defined columns of cells in visual cortex and determine the impact on the spiking responses of neurons using extracellular recordings. This approach revealed cortical interactions that extend over 1 mm in V1. However, within this interaction envelope, we find little evidence for columnar specificity in the locations from which spiking responses are elicited by optogenetic activation. Instead, the strength of the optogenetic activation depends primarily on the distance of the stimulation site from the recording electrode and on the total amount of blue light delivered to the cortex. Regardless of the site of stimulation, activation of horizontal inputs uniformly in-

Received Sept. 25, 2013; revised Jan. 29, 2014; accepted Feb. 27, 2014.

Author contributions: X.H., Y.M.E., W.H.B., and D.F. designed research; X.H., Y.M.E., W.H.B., and T.W. performed research; X.H., Y.M.E., and W.H.B. analyzed data; X.H., Y.M.E., W.H.B., and D.F. wrote the paper.

This work was supported by grants from the U.S. National Institutes of Health to D.F. We thank the Human Frontiers Science Program for providing a fellowship to Y.M.E.. We thank Steve D. Van Hooser and members of the Fitzpatrick laboratory for helpful discussions, and Jiefeng Jiang for MATLAB code for analyzing tuning curves during experiments. We thank the Deisseroth laboratory for the ChR2 construct for AAV virus, and we thank the Boyden laboratory for the lentivirus.

The authors declare no competing financial interests.

*X.H. and Y.M.E. contributed equally to this work.

Correspondence should be addressed to David Fitzpatrick, Max Planck Florida Institute for Neuroscience, 1 Max Planck Way, Jupiter, FL, 33458. E-mail: David.Fitzpatrick@mpfi.org.

DOI:10.1523/JNEUROSCI.4116-13.2014

 0270-6474/14/344976-15$15.00/0

creases responses without change in response gain or visual stimulus tuning functions.

Materials and Methods

Subjects and overview

All experimental procedures were approved by the Duke University Animal Care and Use Committee and the Max Planck Florida Institute Animal Care and Use Committee and performed in compliance with guidelines published by the National Institutes of Health. Tree shrews (*Tupaia belangeri*; $n = 28$, 2–4 months of age, male and female) were injected with a virus expressing Channelrhodopsin2 (ChR2), allowed to recover for a period of weeks, and then used in a terminal experiment that included combinations of optical imaging, optogenetic activation, and electrophysiological recordings.

Viral expression of ChR2

Tree shrews were initially anesthetized with a mixture of ketamine and xylazine (200 mg/kg and 4.7–7.8 mg/kg, i.m.) and given atropine (0.5 mg/kg, s.c.) to reduce secretions. If necessary, anesthesia was extended by gas anesthesia (isoflurane 0.5–1.5% in N_2O/O_2 1:1) delivered through a face mask or endotracheal tube. The animals' heads were shaved and they were placed in a modified stereotaxic device. The surgical site was injected with bupivacaine (0.3–0.5 ml, s.c.). A small incision was made, skin and muscle were retracted, and a small craniotomy was made approximately in the area over the center of the primary visual cortex. One to two microliters of viral solution (1×10^{12}–5×10^{13} GC/ml) containing AAV2/9-CaMKIIa-ChR2-YFP.SV40 or AAV2/9-hSynapsin-ChR2-YFP.SV40 (ChR2; Penn Vector Core) was injected into visual cortex through a glass micropipette (tip size 20–30 μm diameter) using a nanoinjector (WPI) at a depth of 500 μm. After the injection, the scalp incision was closed with 4–0 Ethilon sutures, and Neosporin was applied to the wound margin. A long-acting analgesic (buprenorphine, 0.03 mg/kg, s.c.) was administered either immediately before or after the surgery. The animals were placed on a heating blanket in a small cage to recover from anesthesia. A period of 4–6 weeks was allowed for expression time before optical imaging and electrophysiology experiments.

Preparation for physiology experiments

Anesthesia was induced with a mixture of ketamine and xylazine (200 mg/kg and 4.7–7.8 mg/kg, i.m.) and atropine (0.5 mg/kg, s.c.) was administered to reduce secretions. A tracheostomy was made to deliver gas anesthesia (isoflurane 0.5–2% in N_2O/O_2 1:1) by artificial respiration. The animals' heads were shaved and they were placed in a modified stereotaxic device that did not obstruct the view of the stimulus screen. Body temperature (38°C) was maintained by a thermostatically controlled heating pad and expired CO_2 (3.5–4.5%) and heart rate were monitored for any signs of stress. A 1–2 cm incision was made over the skull near the midline, skin and muscle were retracted, and a craniotomy (4×6 mm) was made centered over the previous site of injection of ChR2 into the primary visual cortex. For optical imaging of intrinsic signals, after removal of the skull, agar (2%) and glass coverslip were applied over the visual cortex. The coverslip was removed for electrophysiological recordings. All wound margins and incisions were treated with bupivacaine (0.3–0.5 ml, s.c.), and ear bars were treated with lidocaine ointment (5%). Contact lenses were placed on the eyes for protection. During electrophysiology experiments, Isoflurane level was decreased to 0.5–1%. Pancuronium bromide (2 mg/kg/h, i.p.) was used as a paralytic to prevent eye movements.

Design of combined optical imaging and optogenetic stimulation equipment

We constructed a wide-field compound microscope that combined intrinsic optical imaging ("imaging arm") with patterned delivery of light ("excitation arm") through the same objective lens. For intrinsic signal imaging, the surface of the brain was illuminated with light from a fiber optic illuminator (Oriel), using tungsten bulbs (USHIO 12 V, 100 W), filtered through both a heat filter and a near-infrared bandpass filter (690 ± 20 nm), and delivered to the brain by external fiber optic cables. The light reflected from the brain was collected in the imaging arm by the objective (Nikon 10×, NA 0.3, WD16, CFI Plan Fluor), filtered by a long-pass dichromatic mirror (>505 nm), and focused with a tube lens onto a CCD camera (Dalsa, model 1M60). Power was adjusted to just below saturation of the camera.

For patterned blue light delivery, light from a mercury arc lamp fed into a liquid light guide (X-Cite; Lumen Dynamics) was collimated into the excitation arm by an aspherical lens, filtered with a bandpass filter (450 ± 25 nm), and passed through a transmissive liquid crystal spatial light modulator (SLM; LC2002, Holoeye) assembly. The SLM was configured to work in the amplitude modulation mode using a broadband laminated polarizer and a corresponding 90°-shifted analyzer (20LP-VIS-B; Newport), allowing direct control of the transmitted power at each pixel by changing the shift of polarization it induces. Light exiting the SLM was collected and collimated by a separate tube lens, reflected onto the back aperture of the objective by the dichromatic mirror and imaged onto the brain. For dual-mode, blue-light stimulation and intrinsic optical imaging acquisition, a bandpass filter was added to the imaging arm after the dichroic mirror (ET700/75 nm). Maximum power at the surface of the brain was 1.5 mW/mm^2 over a rectangular area $\sim 4 \times 6$ mm in size, corresponding to the aperture of the SLM. At zero power setting, residual light leakage was visible but could not be detected using our power meter (<0.02 mW/mm^2).

The SLM patterns were generated by custom-written MATLAB software using the Psychophysics Toolbox and delivered to the SLM using the company's proprietary driver, which addresses the SLM as an external monitor through a serial port. The software was used to register the SLM patterns to the imaging data by projecting patterns and imaging them with the camera. A set of 9–15 points was manually marked on the camera image and on the projected pattern and used to define an affine image transformation using MATLAB's Image Processing Toolbox. This transformation was then used to calculate the SLM patterns based on patterns specified graphically on camera images. Timing was synchronized by external triggers generated by the visual stimulation software.

To image the extent of expression of ChR2-YFP, the excitation arm was used to excite YFP using a 497 ± 16 nm excitation filter, and the emitted light was collected in the imaging arm using a 535 ± 22 nm emission filter.

Optical imaging of intrinsic signals

Our procedures for intrinsic signal imaging have been previously published (Bosking et al., 1997, 2000). Raw data frames were acquired from the camera using the VDAQ software system (Optical Imaging) at a rate of 200 Hz, and every 100 frames was averaged to generate final data frames, each corresponding to 0.5 s. There were 10 final data frames for each 5 s stimulus trial, 0.5 s delay and 4.5 s visual stimulation. In all animals, optical imaging was used to determine the map of orientation preference in V1. For these experiments the visual stimuli were gratings that filled the entire stimulus screen, presented at 100% contrast, spatial frequency (SF) of 0.2 cycles/degree, and temporal frequency (TF) of 4 Hz, presented for a duration of 4.5 s. In some animals, we also used optical imaging to measure the cortical response obtained with blue light stimulation of particular columns of cortex. In these experiments, the blue light was on for 2 s (four frames) of the trial after a 0.5 s delay, and then the intrinsic signal response resulting from this stimulus was examined from the remaining 2.5 s (five frames).

Extracellular recording

We recorded from layer 2/3 neurons (depths: 150–500 μm) with tungsten microelectrodes (1–2 MΩ or 3–4 MΩ; FHC) positioned by a micromanipulator (MP285; Sutter Instrument Company). Multi-unit responses to visual stimuli (1–2 s) or blue light stimulation were acquired using a digital signal acquisition interface (CED; 1401+). Analysis of continuous voltage records and single-unit spike sorting were performed using commercial software (Spike2; CED). Spike records were acquired during the presentation of optogenetic stimulation alone, visual stimulation alone, or combined optogenetic and visual stimulation.

To estimate the final position of the electrode tip on the imaging frame, we calculated a linear transformation between the axes of the SLM microscope (which depended on the spatial orientation of the craniotomy and thus differed between animals) and those of the electrode mi-

cromanipulator. To do this we took two images of the electrode tip at two different positions on the diagonal trajectory of the electrode ("fourth axis") outside of the brain, and used those coordinates on the camera image to linearly extrapolate the location of the electrode in the brain from an image of the tip immediately before penetration into the brain.

For the first recording site in an experiment, we targeted orientation columns in the center of the field of view, while at same time avoiding blood vessels, and we took an image of the electrode tip on the surface of the cortex. We then lowered the electrode until we found visually responsive isolated single-units or multi-unit activity. We obtained an orientation tuning curve for the recording site, and used the preferred orientation (assessed quantitatively) to determine which orientation difference map from the optical imaging experiments to use as the referent for targeted optogenetic stimulation of iso-oriented or orthogonal orientation columns with blue light. Only recording sites that had well defined orientation tuning curves with a single peak were chosen for further analysis. We emphasize that the estimated electrode tip location based on the entry point into the cortex and the angle of penetration of the electrode was not used as the basis for deciding which imaging map to use; rather, we used the estimated electrode tip location based on geometry to display the electrode location in the figures. In all cases, the orientation preference of the recording site was consistent with the orientation preference of the electrode site defined by optical imaging. To confirm the electrode location, we also delivered a small spot of blue light on the center of the orientation column that the electrode was in to confirm that this small spatially restricted stimulus was effective at driving activity from the recording site. For subsequent recording sites, we attempted to target orientation columns with different orientation preferences. Sometimes we used one orientation difference map to guide the electrode to a column with a different orientation, but we always obtained orientation tuning curves from the recording site and used the preferred orientation of the recording site as the basis for selecting columns for blue light stimulation.

Optogenetic activation

There were five basic types of experiments in which we used optogenetic activation alone while recording spiking of layer 2/3 cells: (1) mapping with single spots of blue light, (2) cooperativity between sites using multiple spots, (3) interaction distance, (4) axis specificity, and (5) domain specificity.

In the optogenetic mapping experiments (Fig. 3), three full tessellations of the imaging area were made consisting of hexagons with a diameter of 125 μm or 250 μm (i.e., inscribing circle); the three tessellations were staggered relative to each other by placing the centers of their hexagons on vertices of hexagons in the two other tessellations.

In the cooperative activation experiments (Fig. 5), we used the orientation difference maps to select one orientation column to target with the extracellular electrode. For each recording site, we first obtained an orientation tuning curve to confirm the orientation preference. Then, several columns with similar orientation preference were selected as target sites for optogenetic stimulation, including one centered directly over the recording electrode. Each column was stimulated with a single hexagon ($d = 250$ μm). Five repetitions of all possible combinations of activation of these sites were tested.

To assess cortical interaction distances (Fig. 4), we used two different types of blue light stimuli: (1) circular areas of blue light stimulation that were centered over the recording electrode, and which were gradually increased in size, and (2) large area of blue light stimulation with a circular area over the electrode masked out (we will refer to this as the "inverse circle" stimulus). These circular and inverted circle stimuli were presented with or without a visual stimulus, which was centered over the receptive field (RF) of the recorded cell.

To assess axis specificity of the optogenetic effects (Fig. 10*E*,*F*), orientation domains that matched the orientation preference of the recording site were stimulated in sets that fell along an axis in the cortex corresponding to either the preferred orientation or the orthogonal orientation.

Domain specificity was tested by stimulating sets of columns that were at approximately the same distance from the recording site but which were either the same orientation as the recording site or the orthogonal orientation (Figs. 6, 10*G*,*H*). In some experiments, preferred and orthogonal domains were stimulated in separate trials (Figs. 6*A*,*B*, 10*G*,*H*; $n = 6$), and in other experiments, preferred and orthogonal domains were stimulated randomly interleaved within the same trial (Fig. 6*C–F*; $n = 4$).

Visual stimulation

Visual stimuli were generated on a Macintosh computer using MATLAB and the Psychophysics Toolbox. Stimuli were displayed on a Sony GDM F520 color CRT monitor (40.4 cm wide × 30.2 cm high) with a resolution of 800 × 600 pixels or a LCD monitor (29 cm wide × 51 cm high) with a resolution of 1920 × 1080 pixels. The refresh rate of the monitors was 120 Hz, and the mean luminance was 54 cd/m^2. The stimulus monitor was placed at a distance of 27.6 cm from the eyes. There were two main types of visual stimulation experiments: (1) orientation tuning and (2) length tuning.

Orientation tuning. Square wave gratings drifting in both directions were presented at eight different orientations. The size of the grating was 18 × 18°, centered on the receptive field, with contrast set between 10 and 100%, SF 0.2 cycles/degree, and TF 4 Hz, presented for 2 s. RFs were estimated by manually adjusting the location of panning grating or oriented bar stimuli while listening to amplified voltage recordings, or determined quantitatively by presenting drifting gratings in an array of different spatial locations.

Length tuning. For length tuning experiments, we used square wave gratings presented at the preferred orientation, centered on RF, with stimulus width set at 18°, and stimulus length varying from 4.5 to 40.5°. Contrast was set at one of six different levels (0.1, 0.2, 0.3, 0.5, 0.7, 1.0), SF 0.2 cycles/degree, TF 4 Hz, and stimulus duration was 2 s. Ten stimulus lengths were used and responses to each length were examined with or without simultaneous blue light presentation to activate ChR2 in selected cortical columns.

Viral expression and optogenetic activation used for orientation tuning experiments

In the experiments where we examined the effects of ChR2 activation on orientation tuning curve properties, we used the lentivirus (pLenti-CaMKIIa-hChR2-EYFP-WPRE, titer 1–5 × 10E9 IU/ml) to deliver ChR2 to the visual cortex ($n = 8$). One to two microliters of viral solution was injected into visual cortex through a glass micropipette (tip size 20–30 μm diameter) using a nanoinjector (WPI) at a depth of 500 μm. For five of these animals, we used a 200 μm diameter optical fiber (Thorlabs; BFL22-200) to deliver monochromatic blue light from a 473 nm laser (IkeCool) directly onto the surface of the cortex within the virus expression area (power < 5 mW/mm^2). For three animals, we used the SLM to deliver a single spot of blue light to the cortex as described in the preceding sections. All other surgical and electrophysiological procedures for these experiments were the same as described above.

Pharmacological blocking experiments

To block excitatory synaptic transmission, we injected the AMPA receptor antagonist 2,3-dihydroxy-6-nitro-7-sulfamoyl-benzoquinoxaline-2,3-dione (NBQX, 100 μM) and the NMDA receptor antagonist (2*R*)-amino-5-phosphonopentanoate (APV, 5 mM), ~1–1.5 mm away from the recording electrode through a glass micropipette using the nanoinjector (see above, Viral expression of ChR2). The injection pipettes were beveled and a bee-stinger tip was pulled using a microforge to ensure easy insertion of the pipette and minimal disruption of the tissue. The injector was used to deliver 69 nl/pulse, 4 pulses/min, for 14 min, for a total volume of ~ 3.8 μl. Effectiveness of the blockade was assessed by recording visually evoked activity and orientation tuning curves in each phase of the experiment.

Perfusion and histology

At the end of the experiments, animals received a lethal injection of Nembutal and were perfused transcardially with 0.9% saline, followed by a mixture of 4% paraformaldehyde in 0.1 M phosphate buffer (PB), pH 7.4. For animals with GABA staining, this was followed by 4% paraformaldehyde and 1% glutaraldehyde in 0.1 M PB, pH 7.2. The brain was then removed, postfixed in 4% paraformaldehyde overnight, transferred

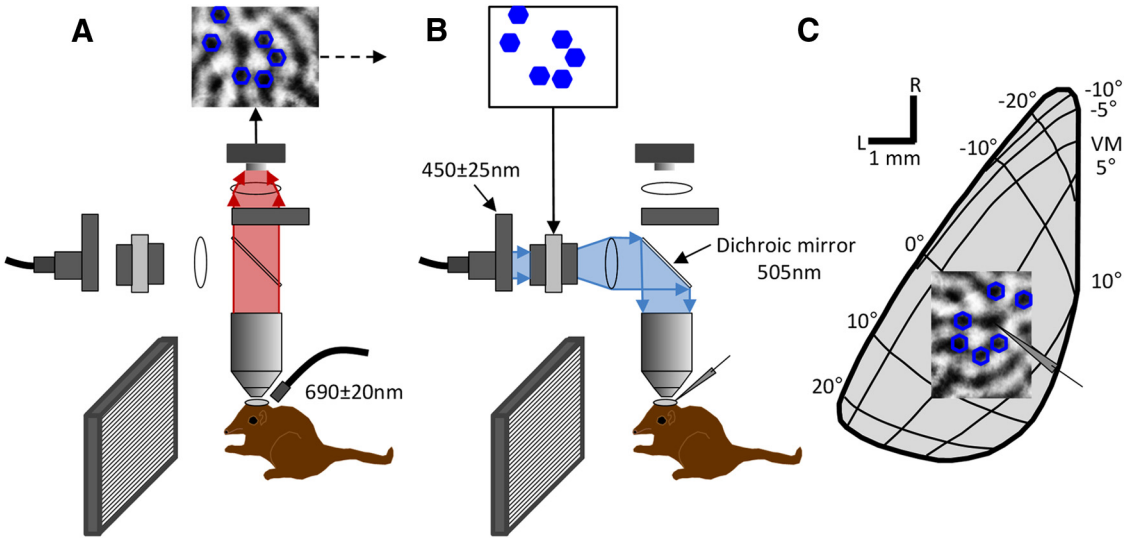

Figure 1. Overview of our experimental design for combined optical imaging, electrophysiology, and optogenetic experiments. ***A***, The first part of the experiment consisting of optical imaging of intrinsic signals is illustrated. The cortex was illuminated with red light (690 ± 20 nm). The optical path (red shading) consisted of a 10× or 4× objective, a dichroic mirror, a lens, and then the CCD camera. Images were acquired while the animal viewed oriented gratings and then orientation difference images were generated. In the difference images (top of figure), dark areas indicate areas of cortex that responded strongly to the grating, and light areas indicate areas that responded to the orthogonal grating. Particular domains from the orientation difference images were selected for ChR2 stimulation with blue light in the next phase of the experiment (blue hexagon outlines on the difference image at the top of the figure). ***B***, Optogenetic activation phase of the experiment. Multi-unit activity was recorded from cells in V1 while the animal was presented with various visual stimuli. In some trials, the cortex was also stimulated by patterns of blue light to activate ChR2. The light path for this phase of the experiment (blue shading) consisted of an Excite light source, a fiber optic cable, a collimating adaptor, a bandpass filter (450 ± 25 nm), a polarizer, the SLM, another polarizer, a lens, the dichroic mirror, and then down through the objective to project the pattern onto the desired domains in visual cortex. ***C***, Schematic indicating the topographic organization of the portion of tree shrew V1 in the left hemisphere located on the dorsal surface and the size and location of a typical recording region for intrinsic signal mapping and optogenetic activation. L, lateral; R, rostral; VM, vertical meridian. The schematic electrode indicates the location of the recorded cell.

to a 20% sucrose solution in the same concentration of PB, and stored at 4°C for 2 d. The area of interest was blocked and then cut on a freezing microtome with 40-μm-thick coronal or tangential sections collected in serial order. For immunostaining, the slices were incubated in blocking solution for 30 min, and then transferred to the primary antibody (rabbit anti-GFP, 1:2000, Invitrogen; guinea pig anti-GABA, 1:500, Millipore) solution for overnight incubation at 4°C. The slices were then incubated in secondary antibody (Alexa 488 anti-rabbit, 1:500; Alexa 594 anti-guinea pig, 1:500; Invitrogen) for 2 h at room temperature and then mounted on glass slides, dried, and coverslipped. Labeled neurons and structures were viewed by a confocal microscope (Zeiss 710 Confocal, 20× objective).

Analysis

Optical imaging data. Data from optical imaging of intrinsic signals experiments typically contained 8–20 repetitions for each of eight orientations. Each trial contained 10 0.5 s time frames. We first subtracted the average image before stimulation (frame 1) from the average image during stimulation (frames 5–9), and averaged over all repetitions. Orientation difference images were then obtained by subtracting the appropriate orthogonal stimulus orientations for each orientation tested. Optical imaging responses to single spots of light were fit with 2D Gaussian curves with seven free parameters [baseline, peak response, location of peak response(x), location of peak response(y), sigmaMajor, sigmaMinor, rotation angle]. The full-width at half-height (FWHH) of the response was calculated by multiplying the average σ by 2.35482.

Electrophysiological data. For all electrophysiology experiments, voltage signals from the electrode were thresholded to obtain multi-unit recordings. In some cases ($n = 5$; Fig. 7), single-unit responses were segregated from multi-unit recordings using template-matching software (Spike2; CED). Single- and multi-unit spike data were analyzed using custom code written in MATLAB. Stimulus responses were assessed using the spikes obtained during the full 2 s visual stimulus period. Background activity was assessed using activity recorded during conditions with no visual or blue light stimulus. Throughout the results, responses from individual example cases are typically presented in terms of the actual spike rate recorded during the experiment. For combining data across different recording sites, we first normalized responses. For analysis of experiments where blue light stimuli were tested alone (Figs. 3–6), normalization was performed by setting the response to one of the blue light conditions to 100%, and scaling all other responses by the same amount. For the mapping (Fig. 3) and interaction distance (Fig. 4) experiments, the response to the condition with the maximum response was set to 100%. For the experiments where different numbers of hexagons were tested (Fig. 5), responses to the condition where a single hexagon was placed over the recording site (center) were set to 100%. For testing of columnar specificity of blue light effects (Fig. 6), responses to stimulation of columns that had the same orientation preference as the recording site were set to 100%, and responses to stimulation of the orthogonal domains were scaled by the same amount. Finally, for analysis of experiments where a visual stimulus as well as a blue light stimulus was used (Figs. 7–10), the responses were normalized such that the response of the site to the most effective visual stimulus was set to 100%. Cortical receptive fields obtained from the hexagon mapping experiments were fit with 2D Gaussian curves as described above for optical imaging data. Spiking responses to the inverted circle stimuli of various sizes were fit with exponential decay curves.

Results

To study functional interactions within layer 2/3 of V1, we designed a wide-field microscope that combines an SLM with an intrinsic optical imaging system (Fig. 1*A*). We injected AAV 2/9-expressing ChR2-YFP under the CaMKIIa or hSyn promoter, or Lentivirus expressing ChR2-YFP under the CaMKII promoter, into primary visual cortex of tree shrews at age 2–4 months, and after a period of 4–6 weeks we performed experiments that combined optical imaging of intrinsic signals, optogenetic activation, and electrophysiological recordings.

Viral expression of ChR2 in visual cortex

Our AAV injections typically resulted in large expression areas, with >50% of the cases yielding expressions areas that were suit-

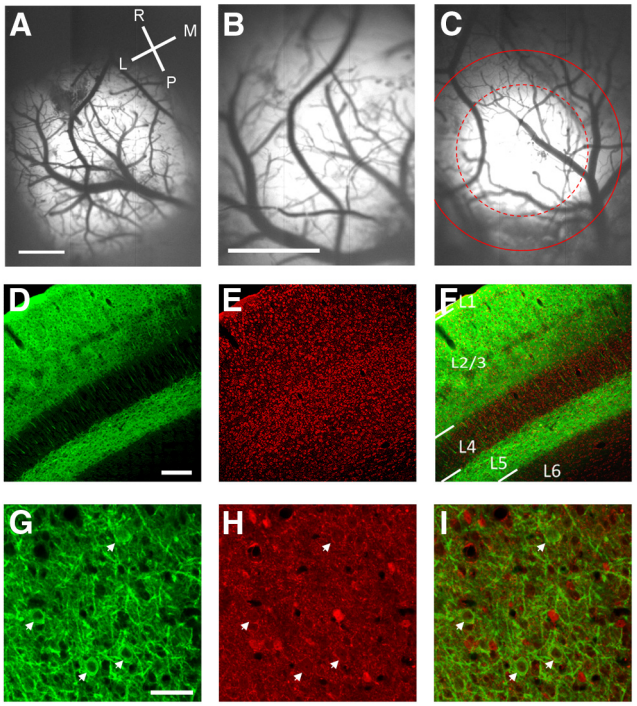

Figure 2. Demonstration of ChR2-YFP expression patterns in V1. ***A***, Example from a case with a very large expression area. Image of YFP expression *in vivo* obtained with the CCD camera through a 4× objective; lighter areas of the image indicate areas with strong ChR2-YFP expression. Scale bar, 1 mm. L, lateral; M, medial; R, rostral; P, posterior. ***B***, Imaging of YFP expression of the same case as shown in ***A*** with the 10× objective typically used for our optical imaging and optogenetic experiments. With this objective the fluorescence appears to fill the entire imaging window. Scale bars: ***B***, ***C***, 1 mm. ***C***, Imaging of YFP from a second case with a more moderate expression area. The dashed red circle indicates the FWHH of the best-fit 2 d Gaussian. The solid red line indicates the full-width at 20% of maximum fluorescence. ***D***, Coronal section of V1 stained for YFP. Staining for cell bodies is strong in the superficial layers and layer 5 and is absent in layer 4. Scale bars: ***D–F***, 200 μm. ***E***, Nissl staining of the same coronal section as shown in ***D***. ***F***, Overlay of the Nissl staining (red) and YFP staining (green). L1, layer 1; L2/3, layer 2/3; L4, layer 4; L5, layer 5; L6, layer 6. ***G***, Tangential section of V1 stained for YFP imaged at high magnification showing the fine pattern of staining within layer 2/3. White arrows show neurons labeled with ChR2. Scale bars: ***G–I***, 50 μm. ***H***, GABA staining of the same section as shown in ***G***; white arrows show that the same neurons in ***G*** are negative with GABA staining. ***I***, Overlay of YFP staining (green) and GABA staining (red).

able for further analysis ($n = 12/21$; Fig. 2). Six of these cases had an expression area that exceeded 2 mm in diameter, or extended beyond our imaging field of view, which was 2 × 3 mm in size (Fig. 2*A*,*B*). For the remaining six, the median diameter of the expression area was 1439 μm, as measured by the FWHH of the YFP fluorescence. The median full-width at 20% of maximum, which seemed to correspond well to the area of cortex that we were able to drive with optogenetic stimulation, was 2193 μm (Fig. 2*C*).

Confocal images of immunostained coronal sections of V1 demonstrated the restriction of ChR2 expression exclusively to neurons in layers 2/3 and layer 5, with little or no labeling in layer 4 (Fig. 2*D–F*). Higher magnification confocal microscopy in tangential sections demonstrated that ChR2-YFP is well localized to the plasma membrane and processes of labeled neurons (Figure 2*G*). To determine the cell-type specificity of labeled neurons obtained when we used the AAV virus under the CaMKIIa promoter, we used the inhibitory neuron-specific marker GABA antibody to immunostain cortical slices obtained from animals with expression of ChR2. Neurons with expression of ChR2-YFP were consistently negative for GABA staining (Figure 2*G–I*; 0/66 cells).

Determining the location of orientation preference domains

Optical imaging of intrinsic signals was used both as a control to determine the normal functioning of V1 with expression of the optogenetic constructs we used, and to determine the location of specific domains in V1 for stimulation. We obtained responses to high-contrast square wave gratings presented at eight different orientations. Orientation difference images were obtained by subtracting data from orthogonal pairs (see Materials and Methods), and were then used to select the sites for electrophysiological recordings and to select specific spatial patterns of blue light that would be delivered by the SLM (Fig. 1*A*). The SLM allowed us to activate single isolated iso-orientation domains, multiple iso-orientation domains of the same orientation preference, or any arbitrary pattern within the expression area. We used these patterns of optogenetic activation, with or without simultaneous presentation of a visual stimulus, to study the range and specificity of lateral interactions within V1 and the effect of lateral activation on the response properties of neurons in layer 2/3. Below, we first present the results where optogenetic activation was used without visual stimulation, and then in later sections we will describe the interactions observed when optogenetic activation and visual stimulation were delivered simultaneously.

ChR2 stimulation results in localized cortical activation

We used two methods to determine the extent and nature of cortical responses evoked by optogenetic stimulation of single domains in V1. First, we combined optogenetic activation with optical imaging of intrinsic signals to measure the evoked cortical response (Fig. 3*A–C*). To ensure that the cortical areas of interest were responsive, we used intrinsic signal imaging to acquire orientation difference maps (Fig. 3*A*,*D*), then a single hexagon of blue light ~250 μm in diameter was delivered to the cortex. To reduce artifacts due to application of blue light during optical imaging, we used a bandpass filter (700 nm/75 nm) placed after the dichroic mirror and before the CCD camera in the imaging path (Fig. 1). However, small artifacts were still visible in early time frames (frames 2–5; time 0.5–2.5 s) while the blue light stimulus was on (Fig. 3*B*,*E*, white areas). We therefore included in the analysis only the data frames collected after the blue light stimulus had been turned off (frames 6–10; time 2.5–5 s). Intrinsic imaging responses were tightly coupled to the location and the size of blue light stimulation (Figure 3*C*). We quantified the spread of activity seen with stimulation of single spots by fitting a 2D Gaussian to the intrinsic signal response. The average FWHH was 450 ± 100 μm (mean ± SD, $n = 8$).

In two control animals that did not receive a virus injection, we could not detect any intrinsic signal responses elicited by blue light (Fig. 3*D–F*). In the example shown in Figure 3, the blue light artifact is still visible in early time frames (Fig. 3*E*, five white spots), but no intrinsic signal response is observed in later time frames (Fig. 3*F*).

The experiments just described demonstrate that we can use a single spot of blue light stimulation to obtain very focal activation in V1. However, because one important goal of our experiments was to test the orientation, or domain, specificity of optogenetic stimulation, we also used intrinsic imaging to validate that we could target multiple spots of blue light stimulation to a specific orientation domain (Fig. 3*G*). In this example, two spots of light were used to stimulate two domains that have the same orientation preference, and the resulting population activity (Fig. 3*H*) closely adhered to the shape of the selected

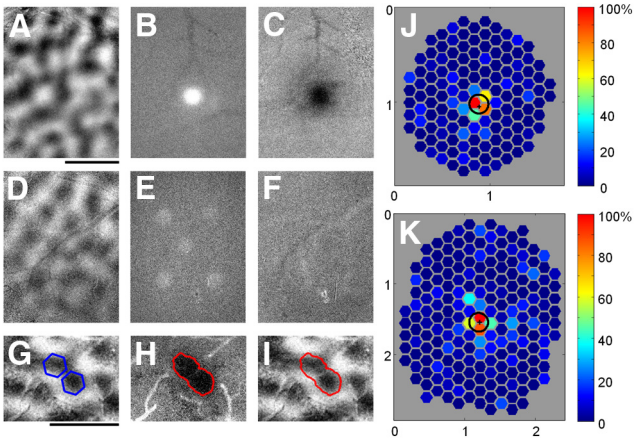

Figure 3. Focal pattern of cortical activity obtained with blue light stimulation demonstrated by intrinsic signal imaging and extracellular recording. ***A–C***, Optical imaging data from a case with ChR2 expression using a blue light stimulus consisting of a single hexagon (edge to edge diameter = 250 μm). ***A***, Orientation difference image. ***B***, Average intrinsic signal response from the 2 s (4 frames) of optical imaging data acquisition while the blue light stimulus was still on. The white area of the image is the direct result of the added blue light during this portion of the trial. ***C***, Average intrinsic signal response from the last 2.5 s (5 frames) of the same trials. The black area indicates the region of cortex that responded strongly to the blue light stimulus. ***D–F***, Optical imaging data from a control case with no ChR2 expression, using a blue light stimulus consisting of five hexagons (diameter = 250 μm). ***D***, Orientation difference map. ***E***, Average intrinsic signal response during the 2 s of blue light stimulation. As in ***B***, the white areas indicate regions where the blue light is being displayed during these frames. ***F***, Average intrinsic signal response during the last 2.5 s (5 frames) of the same trials. There are no dark regions visible, indicating that there was no cortical response to blue light in this control animal. ***G***, Orientation difference map and two sites selected for optogenetic activation with the same orientation preference (blue hexagons). ***H***, Population activity measured in response to activation of the sites shown in ***G***. Red line corresponds to the 50% activation contour. ***I***, The 50% activation contour (red) now placed over the orientation difference image to show focal activation of the selected orientation preference domain. ***J***, ***K***, Electrophysiological recordings used to obtain spatial mapping of cortical areas that provide input to individual recording sites in V1. ***J***, Hexagonal grid showing the response map obtained from a single example case. Each hexagon is centered on one of the sampled cortical locations, and the color of the hexagon shows the average normalized response to blue light presented at that location. Actual hexagons used on each trial were twice as large as those shown in the figure. Strong areas of response are found only within a short range of the electrode ("+" symbol). Black circle indicates the FWHH (199 μm) obtained by fitting a 2D Gaussian curve to the response map. ***K***, The response map and FWHH (266 μm) obtained from a second example case. Scale bars: ***A***, ***G***, 1 mm. Axes labels in ***J*** and ***K*** are in millimeters.

domain (Fig. 3*I*; red contour shown in Fig. 3*H* and *I* corresponds to 50% of maximum response).

The second method we used to map the spatial extent of optogenetic activation in V1 was extracellular recording from a single site, and optogenetic stimulation using single hexagons placed in different locations within the expression area (Fig. 3*J*,*K*). For each recording site, we mapped responses using three complete hexagonal tessellations (d = 250 μm) surrounding the recording site. Each of the three unique tessellations was shifted relative to the other two such that the centers of its hexagons lay on vertices of hexagons in the other two tessellations. For display purposes, the responses are then represented by one collapsed array of half-size hexagons (d = 125 μm) plotted at the center of each original hexagon. The result of this process can be thought of as the cortical response field for blue light stimulation. Two example cortical response fields from two different animals are shown in Figure 3*J* and 3*K*. In these maps, warm colors (yellow and red) represent high activity and cool colors (blue) represent low activity. The black circle on each color plot indicates the 50% response contour from the best-fit 2D Gaussian to the response map for each case (Fig. 3*J*; FWHH = 199 μm; 3*K*; FWHH = 266 μm, mean = 335 ± 236 μm, median = 256 μm, n = 6).

These experiments further demonstrate that the cortical response generated by ChR2 activation of single columns or orientation domains in V1 is spatially restricted. Importantly, we found no evidence for the direct, blue light-driven activation of axonal arborizations which, in L2/3, can extend for several millimeters from the soma. Surprisingly, we saw no evidence for activity driven in neighboring iso-orientation domains with the same orientation preference as the stimulated domain. This would be expected from a connectivity pattern in which neurons in the stimulated domain project preferentially to domains of similar orientation preference and evoke robust responses in these domains.

Cortical summation field defined by ChR2 stimulation

Mapping with small spatially restricted blue light stimuli has the advantage of providing fine-scale topography of the cortical sites that drive responses in a given neuron. However, visually driven activity in layer 2/3 is rarely restricted to such small areas, and it is possible that recruiting a small number of layer 2/3 projections is insufficient to drive postsynaptic neurons to threshold, or that the evoked synaptic responses are too small to result in an intrinsic optical imaging response. Analogous to using small visual stimuli to define the minimum discharge receptive fields of neurons, this approach may underestimate the total area which, when activated simultaneously, can sum together to drive spiking responses. Therefore, to define the cortical summation field, we used two additional sets of stimuli (Fig. 4). The first set was a series of circles of increasing size (Fig. 4*C*,*E*), designed to determine the stimulus size at which an increase in radius no longer produces an increase in spiking response. For the example shown in Figure 4*C*, response reached 75% of maximum at a stimulus size of ~500 μm. On average, the 75% level of response was reached by 390 μm, and 95% of maximum was reached by 720 μm (n = 14).

The second set of stimuli consisted of a large area of blue light stimulation with a circular area centered over the recording site, which was excluded (Fig. 4*D*,*F*). The inner circle was centered over the RF (see Materials and Methods), and the size was varied so that we could measure the radius at which the stimulus no longer produced spiking responses. On average, we found that responses decayed to 50% of maximum by a radius of 350 μm and to 20% of maximum by a radius of 710 μm (n = 14).

To compare the radius of effective cortical interactions measured in these experiments to the physical extent of horizontal connectivity in layer 2/3, we also show here the decay in the density of synaptic contacts made by layer 2/3 cells with increasing distance from the cell body (Fig. 4*F*, black line) using previously published data (Bosking et al., 1997; Chisum et al., 2003). To facilitate this comparison, the values for the two curves were adjusted to be equal at a radius of 200 μm, which was the smallest radius for which the bouton density data are available, but no other adjustments were made to align the two sets of data. Nevertheless, the falloff in bouton density, and the falloff in response magnitude observed in our optogenetic activation experiments appear to be strikingly well correlated.

Synaptic contribution to ChR2 driven summation field

Spiking responses to blue light stimulation can arise from multiple sources including ChR2 channels that are expressed in the recorded neurons, as well as excitatory synaptic inputs from other neurons expressing ChR2. To distinguish the contribution

of direct effects from those requiring excitatory synaptic drive, we recorded activity before, during, and after blockade of excitatory synaptic activity with the AMPAR blocker NBQX and the NMDAR blocker APV (Fig. 4; see Materials and Methods). We monitored spontaneous activity, visually driven activity, and orientation tuning to determine the effectiveness of the blockade. During peak effectiveness of the block, we detected no visually evoked spiking responses (Fig. 4*B*, bottom traces). During this same time period, optogenetic activation was still effective at driving the recording site (Fig. 4*B*, top traces), but spiking responses to both blue light circle and inverted circle stimuli were greatly reduced (Fig. 4*E*,*F*, red lines). Recovery of visually evoked responses and orientation tuning was obtained after waiting ~6–8 h, and at that time the size of the interaction field was measured again (Fig. 4*F*, blue dashed line, $n = 2$).

These results indicate that the impact of ChR2 activation on the responses of the recorded neurons arises largely from synaptic inputs from other neurons, rather than direct stimulation ofChR2 channels in the recorded neuron. Thus, given the average area of dendritic extent in tree shrew V1, direct, light-evoked spiking responses are almost entirely restricted to neurons with cell bodies lying in the area of light delivery, and responses outside of the light delivery area are largely synaptically mediated. Even for the smallest radius of light stimulation that was centered on the location of the recorded neuron, the response to ChR2 stimulation was substantially reduced after synaptic blockade (Fig. 4*E*). Judged by the inverted circle stimulus configuration, beyond a distance of ~300 μm, almost all of the effects of ChR2 activation are synaptically driven.

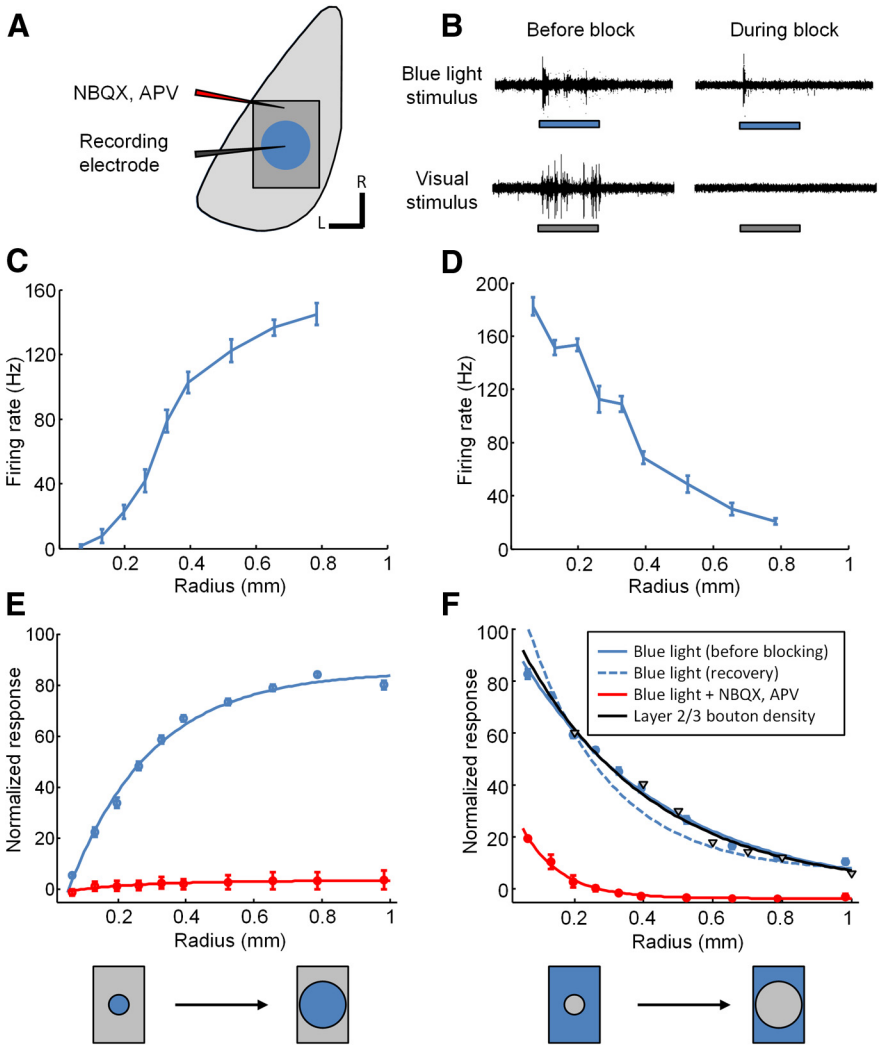

Figure 4. Optogenetic measurement of cortical interaction distances measured with and without blocking of synaptic activity in V1. ***A***, Schematic illustrating the experimental setup. Stimuli consisting of blue light circles of increasing size, or a large blue light stimulus with various portions of the center masked out ("inverted circle" stimuli), were presented centered on the recording location. Recordings were obtained before, during, and after pharmacological blocking of synaptic activity in V1 using NBQX and APV. The pipette used for injection of these drugs was ~1 mm away from the recording electrode. ***B***, Example of multi-unit activity obtained before and during blockade of synaptic activity to optogenetic stimulation (top traces, blue rectangles indicate time of the 2 s blue light stimulus) or to visual stimulation (bottom traces, gray rectangles indicate time of the 2 s visual stimulus). Note the small remaining response to blue light during synaptic blockade (top right) and the total absence of response to visual stimulation during blockade (bottom right). ***C***, Example responses from a single case obtained using blue light stimulation consisting of circles of increasing radius (means with SEM throughout). ***D***, Example responses from the same case for the inverted circle stimuli. ***E***, Average response across all cases for stimuli consisting of blue light circles of increasing radius obtained either before blockade (blue line, $n = 14$), or during blockade (red line, $n = 2$) of synaptic activity. ***F***, Average responses to inverted circle stimuli obtained either before blockade (blue line, $n = 14$) or after recovery from blockade (blue dashed line, $n = 2$) or during blockade (red line, $n = 2$) of synaptic activity. Black line and triangle symbols indicate the average falloff in density of synaptic boutons emanating from horizontal connections in layer 2/3 of tree shrew visual cortex (Bosking et al., 1997; Chisum et al., 2003; Chisum and Fitzpatrick, 2004).

Cooperativity in cortical activation

In the summation experiments described above, the amounts of cortex stimulated, and the distance of the stimulated sites from the recording electrode, were not manipulated independently. In a separate set of experiments we tested whether cortical sites that were located at a moderate distance from the recorded cells, and which were ineffective at driving responses when stimulated in isolation (Fig. 3), would be effective in driving responses when presented in combination with other sites. We delivered blue light to all combinations of iso-orientation columns with preferences matching that of the recording site (Fig. 5). Example results from one recording site are shown in Figure 5*A* and *B*. In this case, the response to blue light stimulation centered directly over the electrode was very strong (Fig. 5*B*, leftmost black circle; ~18 Hz), and the average response to stimulation using a single hexagon centered over one of the surrounding domains without stimulation of the site over the electrode was absent or very weak (Fig. 5*B*, leftmost blue circle). However, a progressive increase in response was seen with addition of more stimulation sites in the surround (Figure 5*B*, blue circles, blue line). The same trend is observed for the overall average across all cases obtained after normalization within each case ($n = 5$; Fig. 5*C*). Summation of responses as more stimulation sites in the surround are added was also observed when the site over the electrode was stimulated simultaneously with activation of the sites in the surround (Fig. 5*B*,*C*, black circles and lines).

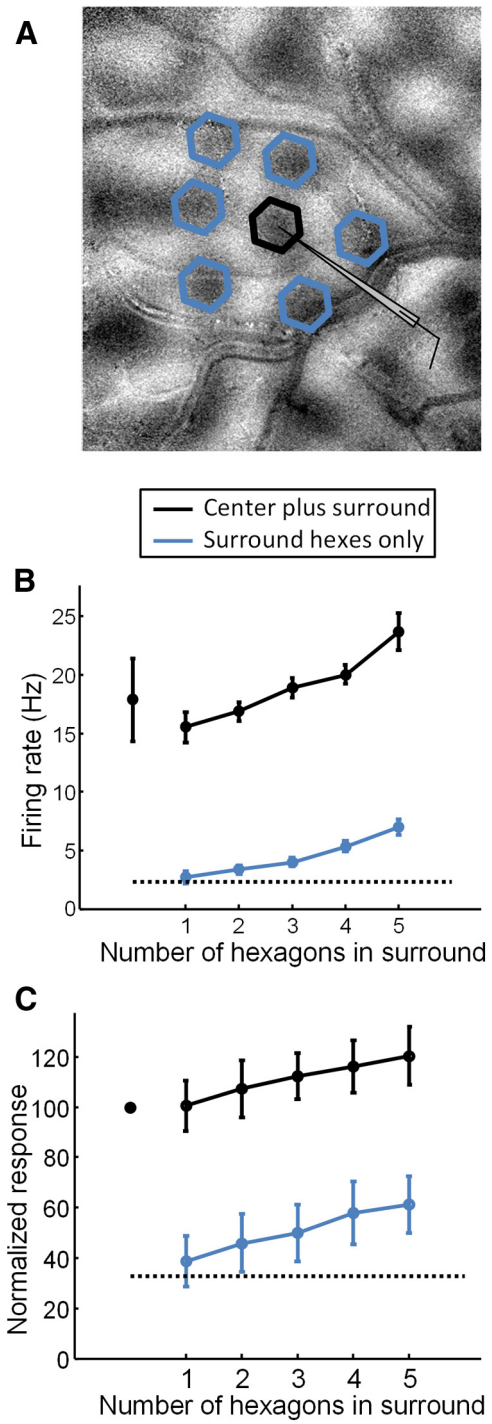

Figure 5. Additive effects obtained by simultaneous presentation of multiple blue light stimuli. ***A***, Orientation difference map, recording site location, and areas that were selected for blue light stimulation in one example case. Hexagons were presented in various combinations centered on orientation domains surrounding the recording site with orientation preference that matched the recording site (blue hexagons) either with or without simultaneous stimulation of the orientation column centered directly over the recording site (black hexagon). ***B***, Multi-unit firing rate obtained from the recording site in ***A*** during blue light stimulation consisting of various combinations of 1–7 hexagons presented at the indicated locations. The black dashed line indicates level of spontaneous activity, leftmost symbol indicates response to the center hexagon alone, blue line indicates response to various number of hexagons in the surround, and black line indicates response to various number of hexagons in the surround while the center hexagon was also present (means with SEM throughout). The data points for combined six hexagons in surround are not shown due to the small sample size. ***C***, Average multi-unit activity obtained from five cases. Labeling conventions same as in ***B***.

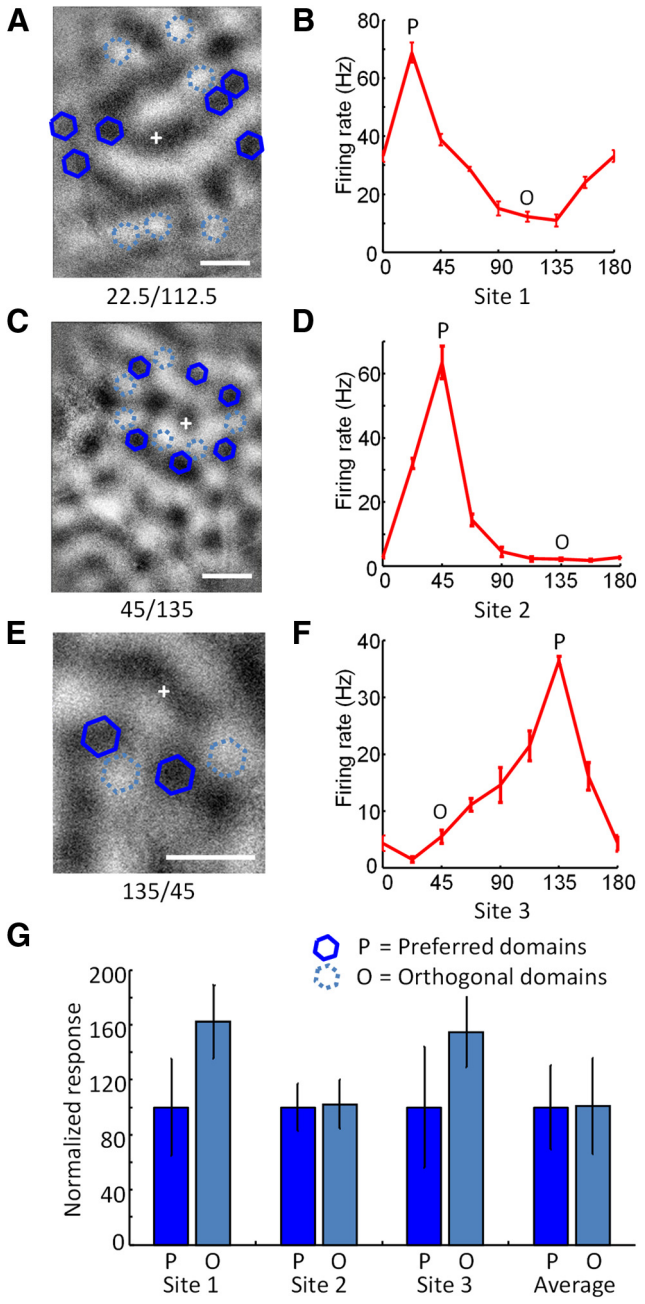

Figure 6. Domain specificity of blue light effects. ***A***, Spatial layout of testing of orientation domain specificity in one case. An orientation difference image is shown with the recording site (+), optogenetic stimulation sites that were centered over orientation domains with the same orientation preference (blue solid hexagons) as the recording site, and stimulation sites that were centered over domains with the orthogonal preference (light blue dashed hexagons). ***B***, Orientation tuning curve from the recording site shown in ***A*** obtained with presentation of visual stimuli of various orientation. Error bars indicate SEM. The preferred orientation is indicated with the letter P, and the orthogonal orientation with the letter O. ***C***, Spatial layout for testing of domain specificity in a second case. ***D***, Orientation tuning curve for the case shown in ***C***. ***E***, Spatial layout for testing of domain specificity in a third case. ***F***, Orientation tuning for the case shown in ***E***. ***G***, Responses to optogenetic stimulation of preferred domains (dark blue) and orthogonal domains (light blue) in the three example cases shown in ***A–F***, and the average responses to stimulation of preferred or orthogonal domains across all cases examined ($n = 10$). Scale bars: ***A***, ***C***, ***E***, 500 μm.

ChR2-driven horizontal inputs lack columnar and axial specificity

Given the anatomical evidence that horizontal connections are biased to columns with similar orientation preference, we designed a series of experiments to determine whether there was a

corresponding bias in the effects of ChR2 stimulation. For each recording site, we first obtained an orientation tuning curve, determined the preferred orientation and the orientation orthogonal to the preferred (Fig. 6*B*,*D*,*F*, P, preferred; O, orthogonal), and then stimulated domains surrounding the recording site corresponding to the preferred orientation (Fig. 6*A*,*C*,*E*, dark blue hexagons), or the orthogonal orientation (Fig. 6*A*,*C*,*E*, dashed blue hexagons) with blue light. The number of stimulated orientation domains was variable (Fig. 6*A*, six sites; *C*, six sites; *E*, two sites), but we attempted to balance both the number of stimulation sites and the distance from the recording site for iso-orientation and orthogonal conditions. While in some individual cases we found larger responses from either iso-orientation or orthogonal-orientation domains (Fig. 6, sites 1 and 3), in other cases we found no difference (Fig. 6, site 2), and when we averaged responses across all recording sites (Fig. 6*G*; $n = 10$) examined we found no consistent bias for larger responses from iso-orientation domains.

The same set of anatomical experiments demonstrates that horizontal connections in the tree shrew also exhibit an axial bias; labeled neurons give rise to more terminals and extend over a greater distance along the axis of preferred orientation (collinear axis) in the map of visual space (Bosking et al., 1997). To determine whether the effects of ChR2 stimulation exhibit a corresponding axial bias, we directed light to several isolated iso-orientation domains that were located on the collinear axis in the cortex or on the orthogonal axis (Fig. 10*E*,*F*; stimulus length = 0°, $n = 7$). We did not find evidence for a bias toward stronger effects with stimulation of sites located on the collinear axis.

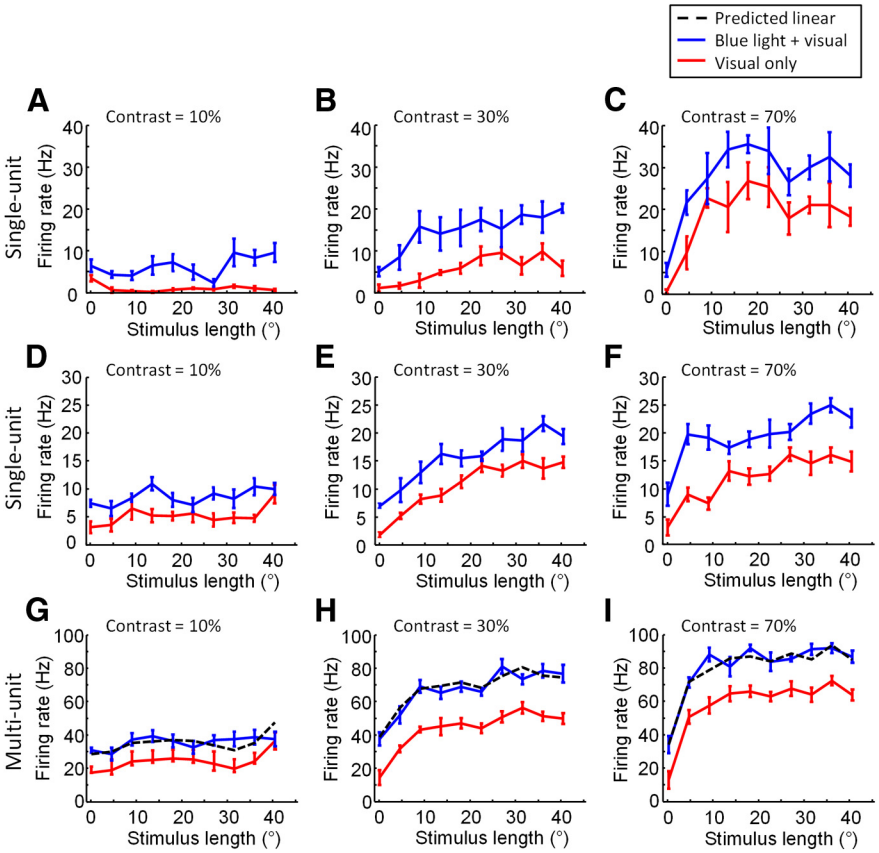

Figure 7. Examples for interaction between blue light stimulation and visual stimulation when parameters of the visual stimulus are varied. ***A–C***, The effect of blue light stimulation on length tuning properties for an example layer 2/3 single-unit recording. ***A***, Length tuning curves obtained with (blue line) and without (red line) simultaneous blue light stimulation. Visual stimulus contrast = 10% (means with SEM throughout). ***B***, Same as in ***A***, but for visual stimulus contrast = 30%. ***C***, Same as in ***A*** and ***B***, but visual stimulus contrast = 70%. ***D–F***, The effect of blue light stimulation on length tuning properties for another example layer 2/3 single-unit recording. ***D***, Visual stimulus contrast = 10%. ***E***, Visual stimulus contrast = 30%. ***F***, Visual stimulus contrast = 70%. ***G–I***, The effect of blue light stimulation on length tuning properties for an example of multi-unit recording, the recording site is the same as in ***D–F***. ***G***, Length tuning curves obtained with (blue line) and without (red line) simultaneous blue light stimulation. Dashed black line indicates the predicted responses to combined visual and optogenetic stimulation if responses added linearly. Visual stimulus contrast = 10%. ***H***, As in ***G***, visual stimulus contrast = 30%. ***I***, As in ***G*** and ***H***, visual stimulus contrast = 70%.

Interaction of optogenetic and visual stimulation of layer 2/3 neurons: Visual stimulus parameters

The effects of ChR2 stimulation described so far have been derived from experiments without simultaneous visual stimulation. It is possible that visual stimulation, which drives layer 4 inputs to layer 2/3 neurons, may impact local cortical circuits in a way that alters the extent, specificity, or the sign (facilitation/suppression) of the effects induced by ChR2 stimulation. Alternatively, blue light stimulation could directly alter the visual response properties of the layer 2/3 neurons that express ChR2. The remaining sections of the results deal with experiments where various combinations of blue light and visual stimulation were used concurrently to examine the range of interactions between these two methods of activating neurons in layer 2/3.

In the first set of experiments, we examined blue light and visual stimulus interactions as we varied the length and contrast of the visual stimulus. The blue light pattern for these experiments was a set of iso-orientation domains with preferences matching the preference of the recording site, at a distance of up to 1.5 mm (example patterns are shown in Figs. 1*C*, 10*C*, example patterns). The visual stimuli consisted of grating patches of various lengths presented at the preferred orientation. In each block, the contrast of the visual stimuli was held constant at one of six values, and 10 different lengths were tested. On half of the trials, blue light stimulation was presented concurrently with visual stimulation. Spiking responses from isolated single units ($n = 5$) to visual stimulation alone (red lines) tended to saturate at medium stimulus lengths when higher contrast stimuli were used (Fig. 7*C*,*F*, contrast = 70%), and at longer stimulus lengths when lower contrast stimuli were used (Fig. 7*B*,*E*, contrast = 30%). However, at all contrast values, the addition of the blue light stimulation (blue lines) caused an increase in response at all stimulus lengths measured, even when the response had saturated by increase in stimulus length alone (Fig. 7*A–F*). Multi-unit responses from single recording sites showed the same characteristics (Fig. 7*G–I*), and were used for all further analyses. Note that the additional spiking response for single-units added by blue light stimulation for visual stimulus conditions

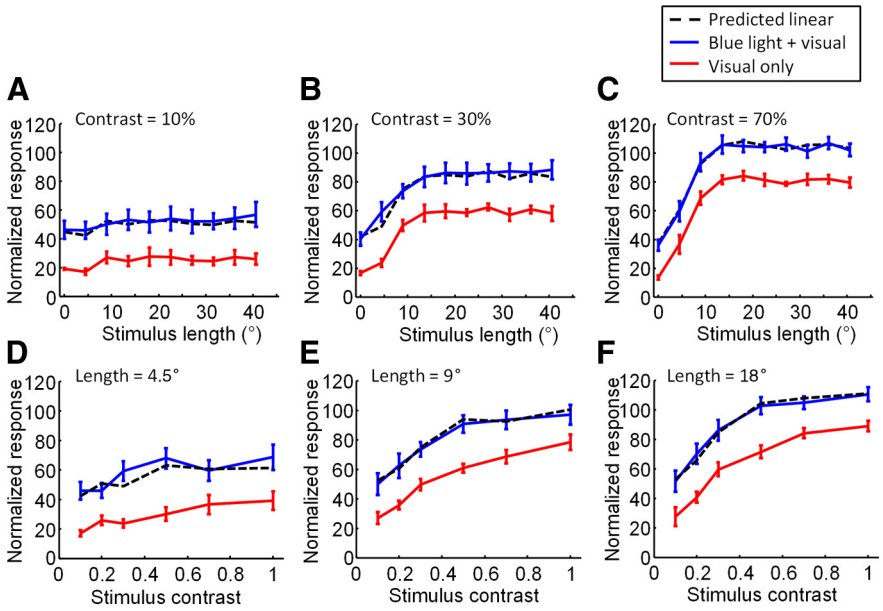

Figure 8. Summary for interaction between blue light stimulation and visual stimulation when parameters of the visual stimulus are varied. ***A–C***, Average effects of blue light stimulation on length tuning properties for the full set of multi-unit recording sites examined ($n = 8$). ***A***, Average length tuning obtained with (blue line) and without (red line) blue light stimulation. Dashed black line indicates the predicted responses to combined visual and optogenetic stimulation if responses added linearly. Visual contrast = 10%. ***B***, Same as in ***A*** but for visual stimulus contrast = 30%. ***C***, Same as in ***A*** and ***B*** but for visual stimulus contrast = 70%. ***D–F***, Average effects of blue stimulation on the contrast tuning properties of the full set of recording sites examined ($n = 8$). ***D***, Average contrast tuning curve either with (blue line) or without (red line) simultaneous blue light stimulation. Dashed black line again indicates prediction if responses added linearly. Visual stimuli were 4.5° in length. ***E***, As in ***D***, but for visual stimuli that were 9° in length. ***F***, As in ***D*** and ***E***, but for visual stimuli that were 18° in length.

where response was already plateaued or saturated by the visual stimulus alone indicates that the blue light effects for these visual stimulus conditions observed for multi-unit recordings was not due solely to the addition of new cells at higher contrast or length values.

Responses from the examples shown in Figure 7 were typical of all cases we examined. To average across cases, we first normalized the multi-unit responses from each case based on the maximum responses obtained to any of the stimulus conditions tested. We then averaged across all cases ($n = 8$) within each condition. Summary data of length tuning with ChR2 activation (blue lines) and without ChR2 activation (red lines) are shown for three particular contrast values in Figure 8*A–C*. Examination of this set of curves reveals a remarkably consistent offset or addition in response obtained by addition of the blue light stimulus. The average response obtained with simultaneous stimulation by blue light and visual stimulation is very well modeled by simple linear addition of the average response to blue light alone and the average response to each particular visual stimulus condition (Fig. 8*A–C*, black dashed lines; $r = 0.9093$, $p < 0.0001$).

The same dataset allows us to examine contrast tuning curves, obtained when the stimulus was set at one of several different lengths, both with and without blue light stimulation (Fig. 8*D–F*). For each visual stimulus length, the responses progressively increased with contrast. Responses to long stimulus lengths approached saturation at high contrast, while responses to shorter stimulus lengths continued to show an increase in response at high contrast. However, addition in response with simultaneous blue light activation was seen for all lengths at all contrasts. Again, the data are well modeled by simple linear addition of the blue light and visual stimulus components (Fig. 8*D–F*, black dashed lines).

In a different set of experiments, we also examined the effects of blue light stimulation on the orientation tuning of layer 2/3 cells. Orientation tuning was tested with eight different oriented gratings, and on half of the trials blue light was used to activate ChR2. Unlike the length tuning and contrast tuning experiments, in this case the pattern of blue light was a single spot, presented by either a fiber optic cable or through the SLM, that was centered on a location within 600 μm of the recording electrode. In some cases, we found that as with the length tuning and contrast data described above, blue light added reliably to all tested orientations in a linear fashion (Fig. 9*A*). In other cases, slight departures from linear addition were observed (Fig. 9*B*). On average, however, as for the length tuning and contrast tuning data described above, we found an increase in response for each orientation, and the average response to combined visual and optogenetic stimulation was well predicted by linear summation of the average visual and average blue light stimulation alone (Fig. 9*C*, black dashed line; $r = 0.9987$, $p < 0.0001$).

Overall, for each combination of the parameters of orientation, length, and contrast, ChR2 stimulation was found to increase the response of layer 2/3 neurons to each visual stimulus such that the shape of the basic tuning function was preserved, altered only by a shift in baseline response equivalent to the response to the ChR2 stimulation alone.

Interaction of optogenetic and visual stimulation of layer 2/3 neurons: blue light parameters

In the experiments presented thus far, we have kept the spatial pattern and level of ChR2 stimulation constant and varied the level of visual drive by changing the contrast, orientation, and length of the visual stimulus. It is possible that the apparent lack of orientation specificity in the interaction between the ChR2 activation of horizontal inputs and visual drive is due to the fact that the horizontal inputs are saturated by the ChR2 stimulation, obscuring the detection of nonlinear interactions that might be evident with reduced ChR2 drive. Therefore, to further evaluate the interaction between ChR2 stimulation and visual drive, we looked at the impact of the activation level of the horizontal network on the response of layer 2/3 neurons to visual stimulation by varying the spatial pattern or intensity of the blue light stimulation in several ways (Fig. 10).

First, we used a blue light stimulus that spanned the entire imaging area, except for a circular area directly centered on the recording electrode, which was not stimulated (Fig. 10*A*). These stimuli were presented with (Fig. 10*B*, dark blue lines) or without a simultaneous presentation of a visual stimulus presented at the preferred orientation (Fig. 10*B*, light blue lines; this is the same data as presented in Fig. 4). Again, in this case, the visual stimulus appears to add a constant to the curve defined by the blue light

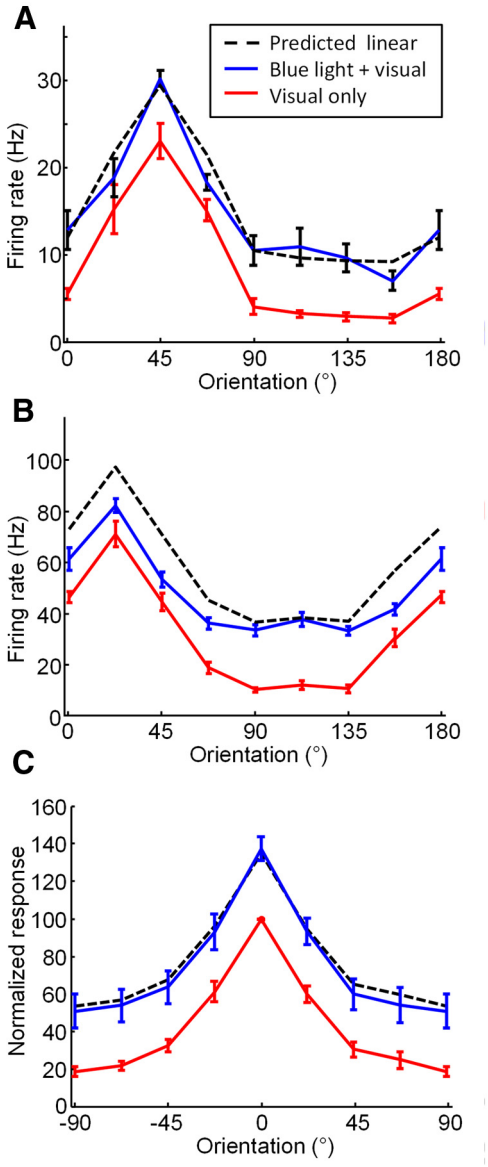

Figure 9. Effects of blue light stimulation on orientation tuning of layer 2/3 cells. ***A***, Orientation tuning from an example recording site obtained with (blue line) and without (red line) simultaneous blue light stimulation. Black dashed line indicates prediction if visual and optogenetic responses add linearly. Error bars indicate SEM. ***B***, A second example site that shows responses that are below that predicted for linear summation. ***C***, Average orientation tuning for all multi-unit recording sites ($n = 16$). Color and line conventions are the same as in ***A–C***.

stimuli, and is well predicted by the linear combination of the two components (black dashed line; $r = 0.9391$, $p < 0.0001$).

We also varied the intensity of the blue light pattern presented to the same spatial pattern of domains (Fig. 10*C*,*D*). These experiments were configured in an identical fashion to the length tuning experiments described earlier, but now separate blocks were run with the blue light illumination for the SLM set at different values. The red lines indicate response to visual stimuli alone, the light blue dashed line indicates response to visual stimulus with blue light at the low setting on the illumination (0.3 mW/mm^2), and the solid blue line indicates response to blue light with visual stimulation when the illumination was on a higher setting (1.25 mW/mm^2). In both cases, the blue light adds a relatively constant amount to the visual response curves, with simply a greater amount added at the higher blue light power setting.

Next, we varied the axis in cortex along which the stimulated domains were arrayed (Fig. 10*E*,*F*). We found that although stimulation along both axes was effective, stimulation along the axis in cortex corresponding to the preferred orientation of the recording site (dark blue line) produced slightly stronger effects than stimulation along the orthogonal axis (light blue dashed line; $n = 7$). However, this pattern of blue light stimulation did not change the basic additive nature of the combined blue light and visual stimulation.

Finally, we varied the spatial pattern of domains stimulated by blue light, with one pattern centered over domains with the same orientation as the recording site, and the other pattern centered over domains with the orthogonal preference (Fig. 10*G*,*H*). We found that stimulation on both domains was effective; stimulation of domains corresponding to the preferred orientation of the recording site (dark blue line; $n = 6$) produced slightly stronger effects than stimulation over the orthogonal domains (light blue dashed line; $n = 6$). However, once again, this pattern of blue light stimulation did not change the basic additive nature of the combined blue light and visual stimulation.

Discussion

Overview

Using spatially patterned optogenetic stimulation of cortical circuits *in vivo*, we characterized the nature and spatial organization of horizontal interactions in visual cortex. We found that optogenetically stimulated horizontal interactions are facilitatory, extend over moderate distances, and arise from columns of similar and dissimilar orientation preference. The effects of optogenetic stimulation sum linearly with visually driven activity over a wide range of variation, without altering cortical tuning properties or network gain.

Cortical interaction distance and sign

Optogenetic stimulation was effective in driving action potentials in layer 2/3 within distances of ~1 mm. Within this distance, we found that progressive increases in the size of a circular illumination field led to progressive increases in response. Moreover, elimination of synaptic transmission reduced the summation distance to ~300 μm, consistent with the view that horizontal connections in layer 2/3 beyond this distance are a source of synaptic inputs that facilitate the response of layer 2/3 neurons. Optogenetic studies performed *in vitro* and *in vivo* in rodents have reported similar cortical interaction distances (Wang et al., 2007; Adesnik and Scanziani, 2010). Given the long distances that horizontal projections extend within layer 2/3 (Rockland et al., 1982; Bosking et al., 1997), we might have predicted interactions to extend over greater distances. However, only ~20% of the terminals of the horizontal network extend beyond a distance of 1 mm, and our results suggest that ChR2 stimulation of the inputs from these distal locations is insufficient to generate action potentials.

Unlike lateral interactions measured in similar experiments performed in layer 2/3 of mouse cortex that were dominated by inhibition (Adesnik and Scanziani, 2010; Adesnik et al., 2012), the effects that we measured with ChR2 stimulation were always facilitatory. Blue light stimulation would not be expected to directly activate GABAergic neurons in our experiments that used the CaMKIIa promoter, but disynaptic effects could have resulted in suppression or reduction in response. It is possible that inhibitory neurons were activated by horizontal activation, but that the net effect of the ChR2 stimulation on population responses remained facilitatory. Also, note that cells in layer 2/3 of tree shrew V1, unlike those in the macaque, cat, or mouse (Levitt and Lund,

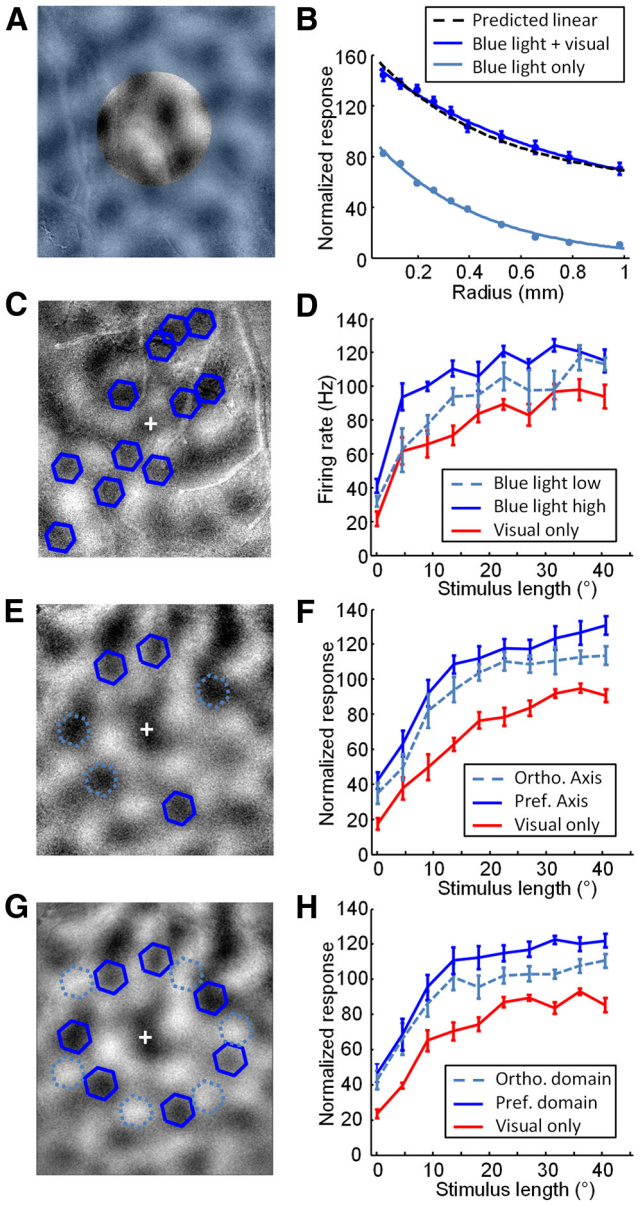

Figure 10. Interaction of blue light stimulation and visual stimulation when parameters of the blue light stimulation are varied. ***A***, Schematic showing the blue light configuration used for testing effects of the size of the blue light stimulation illustrated over an orientation difference map from one case. Blue light stimulation (blue transparent shading) covered the entire imaging area except for a circular central area of variable size centered on the electrode that was not stimulated. ***B***, Average normalized multi-unit recording activity from multiple cases ($n = 14$) using the configuration shown in ***A***, indicating responses to blue light stimulation alone (light blue line) or blue light stimulation with simultaneous visual stimulation (dark blue line). Dashed black line indicates the predicted response if blue light and visual stimulus responses added linearly. Data are from the same cases presented in Figure 4*F*. Error bars indicate SEM. ***C***, Blue light configuration used for testing the effects of blue light intensity. ***D***, Length tuning curves obtained with (blue lines) or without (red lines) simultaneous stimulation of the domains indicated in ***C***, with blue light intensity set at 0.3 mW/mm^2 (light blue dashed line) or 1.25 mW/mm^2 (dark blue solid line). Error bars indicate SEM. ***E***, Configuration used for testing axis specificity of blue light stimulation. An orientation difference image is shown with the multi-unit recording site (+), selected activation sites that are over preferred orientation domains on the preferred axis (dark blue hexagons), and selected activation sites over preferred orientation domains on the orthogonal axis (light blue hexagons, dashed lines). ***F***, Average length tuning results ($n = 7$) with (blue lines) and without (red lines) simultaneous optogenetic activation of the preferred axis (dark blue solid line) or orthogonal axis (light blue dashed line) domains. ***G***, Configuration used for testing domain specificity of blue light stimulation. An orientation difference image is shown with the multi-unit recording site (+), selected activation sites that are over preferred orientation domains (dark blue hexagons), and selected activation sites over orthogonal orientation domains (light blue hexagons, dashed lines). ***H***, Average length tuning results ($n = 6$) with (blue lines) and without (red lines) simultaneous optogenetic activation of the preferred orientation domains (dark blue solid line) or orthogonal orientation domains (light blue dashed line).

1997; Cavanaugh et al., 2002a, b; Bair et al., 2003; Chen et al., 2013; Nienborg et al., 2013), do not exhibit surround suppression. Instead they exhibit continued increase in spiking response to increases in stimulus length (Chisum et al., 2003; Chisum and Fitzpatrick, 2004).

Intercolumnar interactions lack orientation specificity

Within the cortical summation field, the effects of activating columns that had orientation preferences similar to those of the recording site were indistinguishable from the effects of activating those that had the orthogonal preference. This lack of orientation specificity in columnar interactions is surprising given the anatomical evidence for modular specificity in the arrangement of horizontal connections (Gilbert and Wiesel, 1989; Malach et al., 1993; Bosking et al., 1997). It is unlikely that this result can be attributed to a lack of specificity in the ChR2 stimulation method we used. For example, using optical imaging, we found intrinsic signal activity that is localized to the targeted orientation domain. In addition, our mapping experiments using small hexagons showed that significant spiking responses are elicited only by blue light delivered within ~150 μm of the recording site. Finally, blocking excitatory transmission abolished almost all responses to light delivered more than ~300 μm away from the recording electrode. This result indicates that antidromic activation of axons outside this radius does not contribute to the responses we measured under normal conditions.

Some of the nonspecific effects that we observed might be attributable to the pattern of local horizontal connections (within 500 μm) within layer 2/3 that appear to lack modular specificity (Malach et al., 1993; Bosking et al., 1997; Stettler et al., 2002). Thus, specific long range horizontal connections in layer 2/3 may drive nonspecific local layer 2/3 connections resulting in a net nonspecific effect on spiking responses (Fig. 11, red arrows). But it is also conceivable that these nonspecific effects reflect the activation of neurons outside of layer 2/3. For example, layer 5 neurons are likely to be activated by ChR2 stimulation, have extensive axonal projections in layer 2/3 (Fig. 11*A*, purple arrows; Rockland et al., 1982; Gilbert and Wiesel, 1983; Callaway, 1998), and are a significant source of lateral activation (Wester and Contreras, 2012). The degree to which this pathway exhibits functional orientation specificity remains unclear. Feedback connections from V2 (Fig. 11, gray arrow; Stettler et al., 2002) and callosal projections from the opposite hemisphere (Fig. 11, green arrows; Bosking et al., 2000) also appear to lack modular specificity. Overall, our results underscore that monosynaptic horizontal connections are only one of many possible routes through which columnar interactions may be mediated.

Linear summation of optogenetic and visual input

Another prominent feature of our results is that across a wide range of variation in both visual stimulus input and optogenetic input, cortical circuits sum the activity derived from these two sources in a consistently linear fashion. As a result, the shapes of length summation, contrast response, and orientation tuning curves were preserved, and optogenetic stimulation simply in-

duced a constant offset to each visual stimulus condition. In many cases this was true even when the response to visual stimulation alone had reached saturation. Similar additive changes in response magnitude (Fig. 11*C*) have been observed in experiments that selectively activated somatostatin-positive inhibitory neurons in visual cortex (Wilson et al., 2012).

It is important to emphasize that linear addition is only one of many types of interactions that we could have observed. For example, stimulation of layer 2/3 circuits could have modified the gain of the visual response (Fig. 11*D*). Changes in the gain of cortical responses without basic alteration in tuning properties has been observed following selective activation or suppression of layer 6 (Olsen et al., 2012), or silencing of cortical input in mouse visual cortex (Wilson et al., 2012). Another possibility, changes to orientation tuning width (Fig. 11*E*), has also been reported as a result of selective activation of parvalbumin neurons (Lee et al., 2012). Shifts in orientation tuning (Fig. 11*F*), have been observed as a result of local application of GABA (Girardin and Martin, 2009). Finally, combined changes in both the baseline and gain of cortical responses without alteration of tuning properties (Fig. 11*G*) have been observed in multiple experiments (Atallah et al., 2012; Li et al., 2013; Lien and Scanziani, 2013). Interestingly, nonlinear changes, such as changes in the gain of responses for only certain orientations (Fig. 11*H*), or complete disruption of orientation tuning, were possible outcomes that have not been observed.

The linear summation that we observed when a grating stimulus was combined with optogenetic stimulation of orthogonal orientation preference domains is particularly surprising. This combination of stimulation would be expected to produce response normalization as is observed when two orthogonal grating stimuli are displayed simultaneously (Morrone et al., 1982; Bonds, 1989; MacEvoy et al., 2009). This indicates that this feature of cortical circuits may require the activation of layer 4 neurons and GABAergic neurons in layer 2/3 that are not directly activated by ChR2 stimulation in our experiments.

Another aspect of V1 response to visual stimulation that optogenetic stimulation does not appear to induce is the orientation and axis-specific enhancement that is observed in tree shrews and other animals (Knierim and van Essen, 1992; Polat et al., 1998; Chisum et al., 2003; Meirovithz et al., 2010). These physiological effects have been associated with corresponding psychophysiological enhancements in the ability to detect contours (Field et al., 1993; Polat and Sagi, 1994; Kapadia et al., 1995, 1999). The failure to observe collinear enhancement and response normalization highlights some of the future challenges that will be present in using optogenetics for the dissection of circuits *in vivo*, and for the development of neuroprosthetic devices that can produce realistic patterns of cortical activity.

Finally, our results speak to the fundamental question of the contribution of feedforward and recurrent circuits to the response properties of cortical neurons in layer 2/3. The lack of orientation specificity that we observe in horizontal interactions provides evidence that feedforward circuits within a cortical column–in particular those derived from layer 4–are largely responsible for the basic tuning properties that define the column. Patterns of recurrent activity in layer 2/3 appear able to augment or strengthen the level of activity in adjacent columns without altering these properties. This may allow

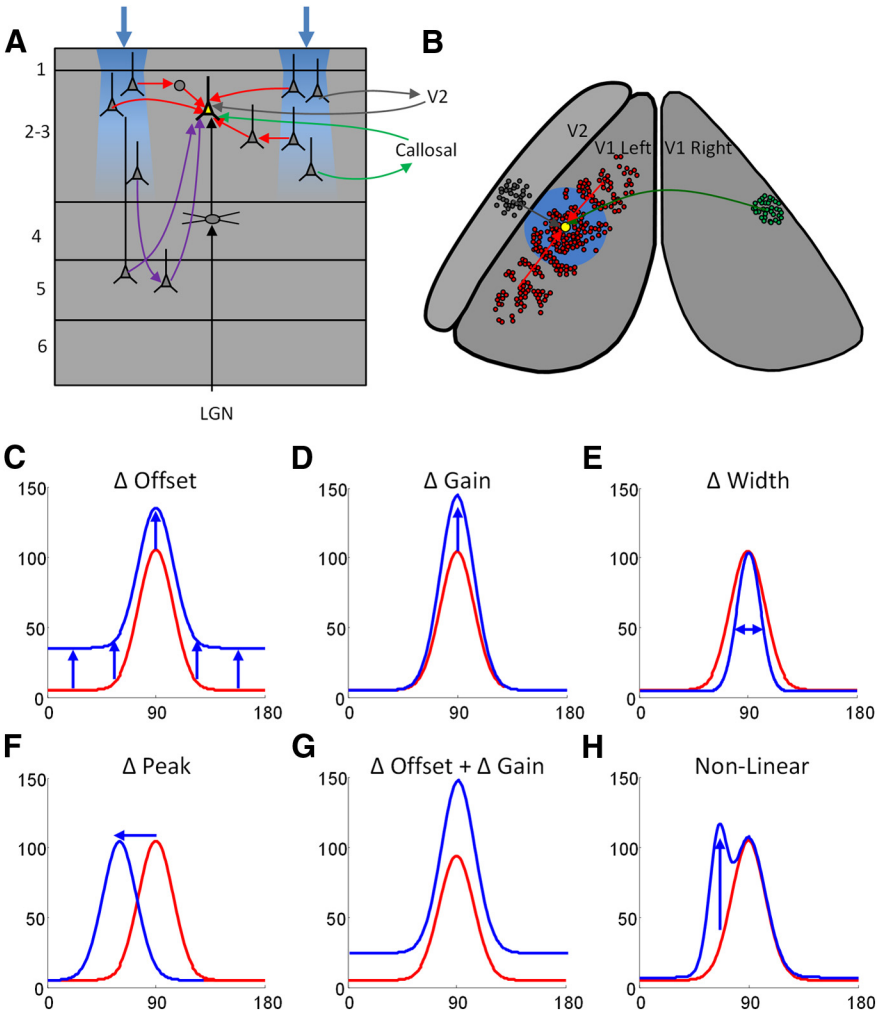

Figure 11. Summary of possible interactions in visual cortex. ***A***, Schematic illustrating a coronal view of V1 and the different types of input that converge on cells in layer 2/3: (1) the retino-geniculo-cortical pathway that provides the primary drive from the visual stimulus (black lines), (2) long distance and local horizontal connections (red lines), (3) input from the opposite hemisphere via the corpus callosum (green lines), (4) input from V2 (gray lines), and (5) input from layer 5 (purple lines). ***B***, Schematic view of the dorsal surface of the visual cortex in both the left and right hemispheres indicating the spatial organization of the inputs shown in ***A***. The recorded cell (yellow) receives input from a dense set of local and long distance horizontal connections (red; Bosking et al., 1997), cells in a topographically corresponding portion of the opposite hemisphere (green), and from cells in V2 (gray). The blue shading indicates the interaction region over which we observed effects of optogenetic stimulation. ***C–H***, Schematics indicating the possible changes to orientation tuning curve that theoretically could have resulted from the addition of optogenetic stimulation in particular orientation domains in V1: (***C***) add an offset, linear addition of optogenetic and visual stimulus responses at all orientations, as observed in our experiments; (***D***) change in response gain or scaling; (***E***) change in tuning width; (***F***) shift in tuning (change in orientation preference); (***G***) combination of change in gain and offset; and (***H***) nonlinear changes, such as selective change in response at specific orientations only.

them to play a critical role in detection of stimuli in low contrast or noisy environments. However, perhaps a more fundamental role for recurrent networks in V1 is suggested by the fact that the interactions that we observe are present even when response to the visual stimulus has saturated. This suggests these circuits could play a role in modulation of V1 responses according to animal state or attention. Further study of the contribution of recurrent circuits in behaving animals will be necessary to evaluate this possibility.

References

Adesnik H, Scanziani M (2010) Lateral competition for cortical space by layer-specific horizontal circuits. Nature 464:1155–1160. CrossRef Medline

Adesnik H, Bruns W, Taniguchi H, Huang ZJ, Scanziani M (2012) A neural circuit for spatial summation in visual cortex. Nature 490:226–231. CrossRef Medline

Atallah BV, Bruns W, Carandini M, Scanziani M (2012) Parvalbumin-expressing interneurons linearly transform cortical responses to visual stimuli. Neuron 73:159–170. CrossRef Medline

Ayling OG, Harrison TC, Boyd JD, Goroshkov A, Murphy TH (2009) Automated light-based mapping of motor cortex by photoactivation of channelrhodopsin-2 transgenic mice. Nat Methods 6:219–224. CrossRef Medline

Bair W, Cavanaugh JR, Movshon JA (2003) Time course and time-distance relationships for surround suppression in macaque V1 neurons. J Neurosci 23:7690–7701. Medline

Bonds AB (1989) Role of inhibition in the specification of orientation selectivity of cells in the cat striate cortex. Vis Neurosci 2:41–55. CrossRef Medline

Bosking WH, Zhang Y, Schofield B, Fitzpatrick D (1997) Orientation selectivity and the arrangement of horizontal connections in tree shrew striate cortex. J Neurosci 17:2112–2127. Medline

Bosking WH, Kretz R, Pucak ML, Fitzpatrick D (2000) Functional specificity of callosal connections in tree shrew striate cortex. J Neurosci 20:2346–2359. Medline

Boyden ES, Zhang F, Bamberg E, Nagel G, Deisseroth K (2005) Millisecond-timescale, genetically targeted optical control of neural activity. Nat Neurosci 8:1263–1268. CrossRef Medline

Callaway EM (1998) Local circuits in primary visual cortex of the macaque monkey. Annu Rev Neurosci 21:47–74. CrossRef Medline

Cavanaugh JR, Bair W, Movshon JA (2002a) Nat and interaction of signals from the receptive field center and surround in macaque V1 neurons. J Neurophysiol 88:2530–2546. CrossRef Medline

Cavanaugh JR, Bair W, Movshon JA (2002b) Selectivity and spatial distribution of signals from the receptive field surround in macaque V1 neurons. J Neurophysiol 88:2547–2556. CrossRef Medline

Chen K, Song XM, Li CY (2013) Contrast-dependent variations in the excitatory classical receptive field and suppressive nonclassical receptive field of cat primary visual cortex. Cereb Cortex 23:283–292. CrossRef Medline

Chisum HJ, Fitzpatrick D (2004) The contribution of vertical and horizontal connections to the receptive field center and surround in V1. Neural Netw 17:681–693. CrossRef Medline

Chisum HJ, Mooser F, Fitzpatrick D (2003) Emergent properties of layer 2/3 neurons reflect the collinear arrangement of horizontal connections in tree shrew visual cortex. J Neurosci 23:2947–2960. Medline

Fenno L, Yizhar O, Deisseroth K (2011) The development and application of optogenetics. Annu Rev Neurosci 34:389–412. CrossRef Medline

Field DJ, Hayes A, Hess RF (1993) Contour integration by the human visual system: evidence for a local "association field". Vision Res 33:173–193. CrossRef Medline

Fitzpatrick D (1996) The functional organization of local circuits in visual cortex: insights from the study of tree shrew striate cortex. Cereb Cortex 6:329–341. CrossRef Medline

Gilbert CD, Wiesel TN (1983) Clustered intrinsic connections in cat visual cortex. J Neurosci 3:1116–1133. Medline

Gilbert CD, Wiesel TN (1989) Columnar specificity of intrinsic horizontal and corticocortical connections in cat visual cortex. J Neurosci 9:2432–2442. Medline

Girardin CC, Martin KA (2009) Inactivation of lateral connections in cat area 17. Eur J Neurosci 29:2092–2102. CrossRef Medline

Harrison TC, Ayling OG, Murphy TH (2012) Distinct cortical circuit mechanisms for complex forelimb movement and motor map topography. Neuron 74:397–409. CrossRef Medline

Hira R, Honkura N, Noguchi J, Maruyama Y, Augustine GJ, Kasai H, Matsuzaki M (2009) Transcranial optogenetic stimulation for functional mapping of the motor cortex. J Neurosci Methods 179:258–263. CrossRef Medline

Hirsch JA, Martinez LM (2006) Circuits that build visual cortical receptive fields. Trends Neurosci 29:30–39. CrossRef Medline

Hubel DH, Wiesel TN (1977) Ferrier lecture. Functional architecture of macaque monkey visual cortex. Proc R Soc Lond B Biol Sci 198:1–59. CrossRef Medline

Kapadia MK, Ito M, Gilbert CD, Westheimer G (1995) Improvement in visual sensitivity by changes in local context: parallel studies in human observers and in V1 of alert monkeys. Neuron 15:843–856. CrossRef Medline

Kapadia MK, Westheimer G, Gilbert CD (1999) Dynamics of spatial summation in primary visual cortex of alert monkeys. Proc Natl Acad Sci U S A 96:12073–12078. CrossRef Medline

Kätzel D, Zemelman BV, Buetfering C, Wölfel M, Miesenböck G (2011) The columnar and laminar organization of inhibitory connections to neocortical excitatory cells. Nat Neurosci 14:100–107. CrossRef Medline

Knierim JJ, van Essen DC (1992) Neuronal responses to static texture patterns in area V1 of the alert macaque monkey. J Neurophysiol 67:961–980. Medline

Lee SH, Kwan AC, Zhang S, Phoumthipphavong V, Flannery JG, Masmanidis SC, Taniguchi H, Huang ZJ, Zhang F, Boyden ES, Deisseroth K, Dan Y (2012) Activation of specific interneurons improves V1 feature selectivity and visual perception. Nature 488:379–383. CrossRef Medline

Levitt JB, Lund JS (1997) Contrast dependence of contextual effects in primate visual cortex. Nature 387:73–76. CrossRef Medline

Li YT, Ibrahim LA, Liu BH, Zhang LI, Tao HW (2013) Linear transformation of thalamocortical input by intracortical excitation. Nat Neurosci 16:1324–1330. CrossRef Medline

Lien AD, Scanziani M (2013) Tuned thalamic excitation is amplified by visual cortical circuits. Nat Neurosci 16:1315–1323. CrossRef Medline

Lim DH, Mohajerani MH, Ledue J, Boyd J, Chen S, Murphy TH (2012) In vivo large-scale cortical mapping using Channelrhodopsin-2 stimulation in transgenic mice reveals asymmetric and reciprocal relationships between cortical areas. Front Neural Circuits 6:11. CrossRef Medline

MacEvoy SP, Tucker TR, Fitzpatrick D (2009) A precise form of divisive suppression supports population coding in the primary visual cortex. Nat Neurosci 12:637–645. CrossRef Medline

Malach R, Amir Y, Harel M, Grinvald A (1993) Relationship between intrinsic connections and functional architecture revealed by optical imaging and in vivo targeted biocytin injections in primate striate cortex. Proc Natl Acad Sci U S A 90:10469–10473. CrossRef Medline

Mao T, Kusefoglu D, Hooks BM, Huber D, Petreanu L, Svoboda K (2011) Long-range neuronal circuits underlying the interaction between sensory and motor cortex. Neuron 72:111–123. CrossRef Medline

Meirovithz E, Ayzenshtat I, Bonneh YS, Itzhack R, Werner-Reiss U, Slovin H (2010) Population response to contextual influences in the primary visual cortex. Cereb Cortex 20:1293–1304. CrossRef Medline

Morrone MC, Burr DC, Maffei L (1982) Functional implications of cross-orientation inhibition of cortical visual cells. I. Neurophysiological evidence. Proc R Soc Lond B Biol Sci 216:335–354. CrossRef Medline

Mountcastle VB (1997) The columnar organization of the neocortex. Brain 120:701–722. CrossRef Medline

Mountcastle VB (2003) Introduction. Computation in cortical columns. Cereb Cortex 13:2–4. CrossRef Medline

Nienborg H, Hasenstaub A, Nauhaus I, Taniguchi H, Huang ZJ, Callaway EM (2013) Contrast dependence and differential contributions from somatostatin- and parvalbumin-expressing neurons to spatial integration in mouse V1. J Neurosci 33:11145–11154. CrossRef Medline

Olsen SR, Bortone DS, Adesnik H, Scanziani M (2012) Gain control by layer six in cortical circuits of vision. Nature 483:47–52. CrossRef Medline

Petreanu L, Huber D, Sobczyk A, Svoboda K (2007) Channelrhodopsin-2-assisted circuit mapping of long-range callosal projections. Nat Neurosci 10:663–668. CrossRef Medline

Petreanu L, Mao T, Sternson SM, Svoboda K (2009) The subcellular organization of neocortical excitatory connections. Nature 457:1142–1145. CrossRef Medline

Polat U, Sagi D (1994) The architecture of perceptual spatial interactions. Vision Res 34:73–78. CrossRef Medline

Polat U, Mizobe K, Pettet MW, Kasamatsu T, Norcia AM (1998) Collinear stimuli regulate visual responses depending on cell's contrast threshold. Nature 391:580–584. CrossRef Medline

Rockland KS, Lund JS, Humphrey AL (1982) Anatomical binding of intrinsic connections in striate cortex of tree shrews (Tupaia glis). J Comp Neurol 209:41–58. CrossRef Medline

Stettler DD, Das A, Bennett J, Gilbert CD (2002) Lateral connectivity and contextual interactions in macaque primary visual cortex. Neuron 36: 739–750. CrossRef Medline

Wang H, Peca J, Matsuzaki M, Matsuzaki K, Noguchi J, Qiu L, Wang D, Zhang F, Boyden E, Deisseroth K, Kasai H, Hall WC, Feng G, Augustine GJ (2007) High-speed mapping of synaptic connectivity using photostimulation in Channelrhodopsin-2 transgenic mice. Proc Natl Acad Sci U S A 104:8143–8148. CrossRef Medline

Wester JC, Contreras D (2012) Columnar interactions determine horizontal propagation of recurrent network activity in neocortex. J Neurosci 32:5454–5471. CrossRef Medline

Wilson NR, Runyan CA, Wang FL, Sur M (2012) Division and subtraction by distinct cortical inhibitory networks in vivo. Nature 488:343–348. CrossRef Medline

Yizhar O, Fenno LE, Davidson TJ, Mogri M, Deisseroth K (2011) Optogenetics in neural systems. Neuron 71:9–34. CrossRef Medline